J|A|C|S
ARTICLES
Published on Web 10/19/2004

Properties of Fullerene[50] and D_{5h} Decachlorofullerene[50]: A Computational Study

Xin Lu,*,†,‡ Zhongfang Chen,*,§ Walter Thiel,|| Paul von Ragué Schleyer,§ Rongbin Huang,† and Lansun Zheng†

Contrbution from the State Key Laboratory of Physical Chemistry of Solid Surfaces & Department of Chemistry, Xiamen University, Xiamen 361005, China, Center for Theoretical Chemistry, Xiamen University, Xiamen 361005, China, Center for Computational Chemistry, The University of Georgia, Athens, Georgia 30602-2525, and Max-Planck-Institut für Kohlenforschung, Kaiser-Wilhelm-Platz 1, D-45470, Mülheim an der Ruhr, Germany

Received June 3, 2004; E-mail: xinlu@xmu.edu.cn; chen@chem.uga.edu

Abstract: Stimulated by the recent preparation and characterization of the first [50]fullerene derivative, decachlorofullerene[50] (*Science* **2004**, *304*, 699), we have performed a systematic density functional study on the electronic and spectroscopic properties of C_{50}, its anions and derivatives such as $C_{50}Cl_{10}$ and $C_{50}Cl_{12}$. The ground state of C_{50} has D_3 symmetry with a spheroid shape, and is highly aromatic; the best D_{5h} C_{50} singlet is nonaromatic. Both D_3 and D_{5h} isomers of C_{50} have high electron affinities and can be reduced easily. Due to the unstable fused pentagon structural features, C_{50} is chemically labile and subject to addition reactions such as chlorination, dimerization and polymerization. The equatorial pentagon−pentagon fusions of D_{5h} C_{50} are active sites for chemical reactions; hence, D_{5h} C_{50} may behave as a multivalent group. The computed IR, Raman, ^{13}C NMR and UV−vis spectra of the D_{5h} $C_{50}Cl_{10}$ molecule agree well with the experimental data. Finally, D_{5h} $C_{50}Cl_{10}$ is predicted to have a high electron affinity and, hence, might serve as an electron-acceptor in photonic/photovoltaic applications. The geometry and ^{13}C NMR chemical shifts of $C_{50}Cl_{12}$ were computed to assist further isolation experiments.

Introduction

The discovery of C_{60} and other fullerenes[1] has led to their consideration[2,3] as new agents and materials for molecular electronics, nanoprobes, superconductors, and nonlinear optics. The properties of fullerenes, as opposed to graphite, are due to the curvature imposed by the presence of pentagons.[4] While fullerenes smaller than C_{60} have been sought actively,[3,5−7] they must have strained pentagon−pentagon fusions,[4] which results in rather high lability. As a result, bulk synthesis of smaller fullerenes has proven to be extremely difficult.[8,9]

In 1998, Zettl's group claimed the first preparation of C_{36}.[6] However, their bulk substance was not molecular C_{36}, but aggregated material.[1b] Actually, the nature of the "C_{36}-based solid" is in doubt, since sp^3 hybridized carbon signals were not found in the ^{13}C NMR spectrum. Moreover, various attempts to reproduce the production of C_{36} by arc-discharge failed.[8] Subsequent theoretical investigations also revealed that molecular C_{36} should be unstable and prone to polymerize.[10] Stimulated by Zettl's work, Shinohara et al. prepared several derivatives of C_{36},[8] but their structural characterization is not available to date. An exciting achievement was the gas-phase generation of C_{20}, the smallest possible fullerene, in 2000.[7] Moreover, its crystallized solid was claimed to have been prepared recently in the ultrahigh molecular weight polyethylene

† State Key Laboratory of Physical Chemistry of Solid Surfaces & Department of Chemistry, Xiamen University.
‡ Center for Theoretical Chemistry, Xiamen University.
§ Center for Computational Chemistry, The University of Georgia.
|| Max-Planck-Institut für Kohlenforschung.

(1) Kroto, H. W.; Heath, J. R.; O'Brien, S. C.; Curl, R. F.; Smalley R. E. *Nature* **1985**, *318*, 162. (b) Kadish, K. M., Ruoff, R. S., Eds. *Fullerene: Chemistry, Physical and Technology*; John Wiley & Sons: New York, 2002. (c) Andreoni, W., Ed. *The Physics of Fullerene-Based and Fullerene-Related Materials*; Kluwer: Dordrecht, 2000. (d) Hirsch, A. *The Chemistry of the Fullerenes*; Thieme: Stuttgart, 1994. (e) Hirsch, A. *Top. Curr. Chem.* **1998**, *199*, 1.
(2) Holczer, K.; Klein, O.; Huang, S. M.; Kaner, R. B.; Fu, K. J.; Whetten, R. L.; Diederich, F. *Science* **1991**, *252*, 1154. (b) Pekker, S.; Janossy, A.; Mihaly, L.; Chauvet, O.; Carrard, M.; Forro, L. *Science* **1994**, *265*, 1077. (c) Lappas, A.; Prassides, K.; Vavekis, K.; Arcon, D.; Blinc, R.; Cevc, P.; Amato A.; Feyerherm, R.; Gygax, F. N.; Schenck, A. *Science* **1995**, *267*, 1799. (d) Kelly, K. F.; Sarkar, D.; Hale, G. D.; Oldenburg, S. J.; Halas, N. J. *Science* **1996**, *273*, 1371. (e) Hornbaker, D. J.; Kahng, S. J.; Misra, S.; Smith, B. W.; Johnson, A. T.; Mele, E. J.; Luzzi, D. E.; Yazdani, A. *Science* **2002**, *295*, 828. (f) Dinnebier, R. E.; Gunnarsson, O.; Brumm, H.; Koch, E.; Stephens, P. W.; Huq, A.; Jansen, M. *Science* **2002**, *296*, 109. (g) Mickelson, W.; Aloni, S.; Han, W. Q.; Cumings, J.; Zettl, A. *Science* **2003**, *300*, 467.
(3) Kroto, H. W. *Nature* **1987**, *329*, 529.
(4) Fowler, P. W.; Manolopoulos, D. E. *An Atlas of Fullerenes*; Clarendon: Oxford, 1995.
(5) Guo, T.; Diener, M. D.; Chai, Y.; Alford, M. J.; Haufler, R. E.; McClure, S. M.; Ohno, T.; Weaver, J. H.; Scuseria, G. E.; Smalley, R. E. *Science* **1992**, *257*, 1661.
(6) Piskoti, C.; Yarger, J.; Zettl, A. *Nature* **1998**, *393*, 771. (b) Heath, J. R. *Nature* **1998**, *393*, 730.
(7) Prinzbach, H.; Weller, A.; Landenberger, P.; Wahl, F.; Worth, J.; Scott, L. T.; Gelmont, M.; Olevano, D.; Issendorff, B, v. *Nature* **2000**, *407*, 60−63.
(8) Koshio, A.; Inakuma, M.; Sugai, T.; Shinohara, H. *J. Am. Chem. Soc.* **2000**, *122*, 398. (b) Koshio, A.; Inakuma, M.; Wang, Z. W.; Sugai, T.; Shinohara, H. *J. Phys. Chem. B* **2000**, *104*, 7908.
(9) Wang, Z.; Ke, X.; Zhu, Z.; Zhu, F.; Ruan, M.; Chen, H.; Huang, R.; Zheng, L. *Phys. Lett. A* **2001**, *280*, 351−356.
(10) Fowler, P. W. Heine, T.; Rogers K. M.; Sandall, J. P. B.; Seifert, G.; Zerbetto, F. *Chem. Phys. Lett.* **1999**, *300*, 369. (b) Fowler, P. W.; Heine, T. *J. Chem. Soc., Perkin Trans. 2* **2001**, 487. (c) Fowler, P. W.; Mitchell, D.; Zerbetto, F. *J. Am. Chem. Soc.* **1999**, *121*, 3218.

samples during Ar^+ ion beam irradiation,[9] but no definite structural assignment is available. A theoretical study aimed to assist characterization of this solid has been performed.[11] Hence, the science of the smaller fullerenes is still in its infancy. The exploration and application of the anticipated properties of smaller fullerenes awaits their bulk syntheses.

Besides C_{60} and C_{70}, C_{50} was also observed as a magic cluster with enhanced intensity in mass spectroscopy in the Nobel-Prize-winning work.[1a] While C_{60} and C_{70} are now readily available[12] and have been investigated extensively,[1b,c] very little is known about C_{50} experimentally. C_{50} has a completely filled electron shell conforming to Hirsch's $2(N + 1)^2$ electron-counting rule for spherical molecules[13] and thus is expected to be highly aromatic; moreover, it is the smallest carbon cage without three directly or sequentially fused pentagons, and should have less strain energy than other smaller fullerenes.[3] The expected high aromaticity and smaller strain energy distinguish C_{50} from other smaller fullerenes. Accordingly, C_{50} has been long considered to be the best preparation prospect for fullerenes smaller than C_{60}.[3,6b] Unfortunately, experimental attempts failed to achieve C_{50} until very recently. Using a modified graphite arc-discharge method,[14] Xie et al. successfully prepared the first C_{50} derivative, decachlorofullerene[50] ($C_{50}Cl_{10}$), in milligram quantities.[15] By means of MS/MS (multiple staged mass spectrum), ^{13}C NMR (nuclear magnetic resonance), IR (infrared), Raman, UV−vis (ultraviolet−visible absorption) and DFT (density functional theory) calculations, it was demonstrated convincingly that this new compound has a D_{5h} fullerene[50] structure with 10 chlorine atoms attached to the equatorial pentagon−pentagon fusions.[15] However, many questions are still unsolved: What is the ground state of C_{50}? What are its electronic and chemical properties? Why was C_{50} itself not obtained in bulk, rather than only its decachloro-derivative? Why are the Cl atoms attached solely to the equatorial sites of C_{50} (D_{5h})? We now address these questions by density functional computations in order to enhance understanding of the unusual chemical properties of smaller fullerenes and to assist further experimental investigations.

Computational Details

The semiempirical MNDO method[16] implemented in the Vamp 7.0 program[17] was used to optimize all possible 271 isomers of [50] fullerene.[4] The reliability of semiempirical methods applied to computational fullerene chemistry has been demonstrated recently.[18] The six lowest energy isomers of C_{50} obtained at MNDO were chosen for higher level studies.

The geometries and electronic structures of D_{5h} and D_3 C_{50}^{q-} ($q = 1$, 2, and 6), C_{50} (D_{5h}) and C_{50} (D_3) dimers, $C_{50}Cl_{10}$ (D_{5h}), $C_{50}Cl_{12}$ (D_3) and other fullerene derivatives were computed at B3LYP/6-31G*. NMR chemical shielding values of C_{50}^{q-} ($q = 0$, 2 and 6) and $C_{50}Cl_n$ ($n = 10$, 12) were evaluated at the same level employing GIAO (gauge-independent atomic orbital) method and the optimized geometries. The ^{13}C chemical shifts of the neutral C_{50}, its dianions and adducts were calculated relative to C_{60} and converted to the TMS scale using the experimental value for C_{60} ($\delta = 142.5$ ppm),[19a,b] while the ^{13}C chemical shifts of the C_{50} hexaanions were referenced to C_{60}^{6-} ($\delta = 156.7$ ppm).[19c] Earlier studies[20] have shown that reasonably accurate computations of fullerene ^{13}C NMR chemical shifts can be expected at density functional levels. The NICS (nucleus-independent chemical shifts)[21] at the cage centers were calculated to evaluate the aromaticity of C_{50} and their derivatives. Vibrational frequencies of $C_{50}Cl_{10}$ were calculated at the B3LYP/6-31G* level with a scaling factor of 0.98.[22] TD-DFT[23] computations on 100 excited states of $C_{50}Cl_{10}$ was carried out at the BP86/3-21G level using the B3LYP/6-31G* optimized geometry. All computations were performed using the Gaussian98 program.[24]

Results and Discussion

1. Ground state of C_{50}. Table 1 summarizes the B3LYP/6-31G* energy data of the low-lying states of C_{50} (see Supporting Information for their optimized structures and the MNDO energies of all possible isomers). We found the singlet D_3 [25] to be the lowest-energy isomer, followed by the two $^1A_1'$ electronic states of the D_{5h} isomer[25,26] (2.3 and 5.6 kcal/mol higher in energy, respectively). Moreover, the D_3 isomer has the largest HOMO−LUMO gap (2.27 eV). Note that D_3 and D_{5h} isomers are the only two C_{50} fullerene isomers without three pentagons directly or sequentially fused; they only have isolated and double pentagon configurations. Exactly, there are six and five pentagon−pentagon fusions within the D_3 and D_{5h} isomers, respectively.

(11) Chen, Z.; Heine, T.; Jiao, H.; Hirsch, A.; Thiel, W.; Schleyer, P. v. R. *Chem. Eur. J.* **2004**, *10*, 963−970.
(12) Krätschmer, W.; Lamb, L. D.; Fostiropoulos, K.; Huffman, D. R. *Nature* **1990**, *347*, 354. (b) Scott, L. T.; Boorum, M. M.; McMahon, B. J.; Hagen, S.; Mack, J.; Blank, J.; Wegner, H.; Meijere, A. de *Science* **2002**, *295*, 1500.
(13) Hirsch, A.; Chen, Z.; Jiao, H. *Angew. Chem., Int. Ed.* **2000**, *39*, 3915. (b) Chen, Z.; Jiao, H.; Hirsch, A.; Thiel, W. *J. Mol. Model.* **2001**, *7*, 161. (c) Hirsch, A.; Chen, Z.; Jiao, H. *Angew. Chem., Int. Ed.* **2001**, *40*, 2834. (d) Chen, Z.; Jiao, H.; Hirsch, A.; Schleyer, P. v. R. *Angew. Chem Int. Ed.* **2002**, *41*, 4309. (e) Chen, Z.; Hirsch, A.; Nagase, S.; Thiel, W.; Schleyer, P. v. R. *J. Am. Chem. Soc.* **2003**, *125*, 15507. (f) for review, see Chen, Z.; Jiao, H.; Hirsch, A. *Spherical aromaticity- an overview, in Fullerenes: From Synthesis to Optoelectronic Properties*; Guldi, D. M., Martin, N., Eds.; Kluwer Academic Publishers: 2002; p 121−135.
(14) Gao, F.; Xie, S. Y.; Huang, R. B.; Zheng, L. S. *Chem. Commun.* **2003**, 2676.
(15) Xie, S. Y.; Gao, F.; Lu X.; Huang, R. B.; Wang, C. R.; Zhang, X.; Liu, M. L.; Deng, S. L.; Zheng, L. S. *Science* **2004**, *304*, 699.
(16) Dewar, M. J. S.; Thiel, W. *J. Am. Chem. Soc.* **1977**, *99*, 4899.
(17) Clark, T.; Alex, A.; Beck, B.; Chandrasekhar, J.; Gedeck, P.; Horn, A.; Hutter, M.; Martin, B.; Rauhut, G.; Sauer, W.; Schindler, T.; Steinke, T. VAMP 7.0; Erlangen 1998.
(18) Chen, Z.; Thiel, W. *Chem. Phys. Lett.* **2003**, *367*, 15.
(19) Taylor, R.; Hare, J. P.; Abdul-Sada, A. K.; Kroto, H, W. *J. Chem. Soc. Chem. Comm.* **1990**, 1423. (b) Taylor, R.; Langley, G. J.; Avent, A. G.; Dennis, T. J. S.; Kroto, H. W.; Walton, D. R. M. *J. Chem. Soc., Perkin Trans. 2* **1993**, 1029. (c) Bausch, J. W.; Prakash, G. K. S.; Olah, G. A.; Tse, D. S.; orents, D. C.; Bae, Y. K.; Malhorta, R. *J. Am. Chem. Soc.* **1991**, *113*, 3205.
(20) Sun, G.; Kertesz, M.; Miklos, *J. Phys. Chem. A* **2000**, *104*, 7398. (b) Sun, G.; Kertesz, M.; Miklos, *J. Phys. Chem. A* **2001**, *105*, 5212. (c) Sun, G.; Kertesz, M. *J. Phys. Chem. A* **2001**, *105*, 5468. (d) Sun, G.; Kertesz, M. *Chem. Phys.* **2002**, *276*, 107. (e) Sun, G. *Chem. Phys. Lett.* **2003**, *367*, 26. (f) Sternfeld, T.; Thilgen, C.; Chen, Z.; Siefken, S.; Schleyer, P. v. R.; Thiel, W.; Diederich, F.; Rabinovitz, M. *J. Org. Chem.* **2003**, *68*, 4850.
(21) Schleyer, P. v. R.; Maerker, C.; Dransfeld, A.; Jiao, H.; Hommes, N. J. R. v. E. *J. Am. Chem. Soc.* **1996**, *118*, 6317.
(22) Stratmann, R. E.; Scuseria, G. E.; Frisch, M. J. *J. Raman Spectrosc.* **1998**, *29*, 483.
(23) Casida, M. E.; Jamorski, C.; Casida K. C.; Salahub, D. R. *J. Chem. Phys.* **1998**, *108*, 4439.
(24) Frisch, M. J.; Trucks, G. W.; Schlegel, H. B.; Scuseria, G. E.; Robb, M. A.; Cheeseman, J. R.; Zakrzewski, V. G.; Montgomery, J. A., Jr.; Stratmann, R. E.; Burant, J. C.; Dapprich, S.; Millam, J. M.; Daniels, A. D.; Kudin, K. N.; Strain, M. C.; Farkas, O.; Tomasi, J.; Barone, V.; Cossi, M.; Cammi, R.; Mennucci, B.; Pomelli, C.; Adamo, C.; Clifford, S.; Ochterski, J.; Petersson, G. A.; Ayala, P. Y.; Cui, Q.; Morokuma, K.; Malick, D. K.; Rabuck, A. D.; Raghavachari, K.; Foresman, J. B.; Cioslowski, J.; Ortiz, J. V.; Stefanov, B. B.; Liu, G.; Liashenko, A.; Piskorz, P.; Komaromi, I.; Gomperts, R.; Martin, R. L.; Fox, D. J.; Keith, T.; Al-Laham, M. A.; Peng, C. Y.; Nanayakkara, A.; Gonzalez, C.; Challacombe, M.; Gill, P. M. W.; Johnson, B. G.; Chen, W.; Wong, M. W.; Andres, J. L.; Head-Gordon, M.; Replogle, E. S.; Pople, J. A. Gaussian 98; Gaussian, Inc.: Pittsburgh, PA, 1998.
(25) Xu, W. G.; Wang, Y.; Li, Q. S. *J. Mol. Struct. (THEOCHEM)* **2000**, *531*, 119.
(26) Bühl, M.; Thiel, W. *Chem. Phys. Lett.* **1995**, *233*, 585. (b) Bühl, M. *Chem. Eur. J.* **1998**, *4*, 734. (c) Chen, Z.; Jiao, H.; Bühl, M.; Hirsch, A.; Thiel, W. *Theor. Chem. Acc.* **2001**, *106*, 352.

Table 1. Relative Energies (E_{Rel}, kcal/mol), HOMO and LUMO Energies and HOMO−LUMO Gap Energies (eV) of the Low-Lying States of C_{50},[a] Its Anions, Its Magnesium Endohedral Complexes and $C_{50}Cl_{10}$ at B3LYP/6-31G* Level

isomer	state	E_{rel} [b]	E_{HOMO}	E_{LUMO}	gap	VEA[d]	AEA[d]
C_{50} 260 (C_2)	^1A	22.7	−5.47	−3.98	1.49		
C_{50} 262 (C_s)	$^1A'$	24.7	−5.60	−3.98	1.63		
C_{50} 264 (C_s)	$^1A'$	18.1	−5.72	−4.10	1.61		
C_{50} 266 (C_s)	$^1A'$	8.1	−5.68	−3.91	1.77		
C_{50} 270 (D_3)	^1A	0.0	−6.01	−3.74	2.27	2.97	3.05
C_{50} 271 (D_{5h})	$^1A_1'$ (A)[c]	5.6	−5.43	−4.16	1.27	3.37	3.51
C_{50} 271 (D_{5h})	$^1A_1'$ (B)[d]	2.3	−5.54	−4.17	1.37	3.40 (3.35)[e]	3.47
C_{50} 271 (D_{5h})	$^3A_2'$	6.8	−5.31	−4.32	0.99		
C_{50}^- 270 (D_3)	^2A	6.9 (7.0)[d]	−1.14	−0.21	0.93		
C_{50}^- 271 (D_{5h})	$^2A_2'$	2.1 (3.2)[d]	−1.79	−0.78	1.01		
C_{50}^- 271 (D_{5h})	$^2A_1'$	0.0 (0.0)[d]	−1.68	−0.75	0.93		
C_{50}^{2-} 270 (D_3)		18.6	2.18	3.61	1.43		
C_{50}^{2-} 271 (D_{5h})		0.0	1.72	3.84	2.12		
Mg@C_{50} 270 (D_3)		27.6	−4.88	−4.62	0.26		
Mg@C_{50} 271 (D_{5h})		0.0	−5.54	−4.01	1.53		
C_{50}^{6-} 270 (D_3)		−6.0	15.75	18.28	2.53		
C_{50}^{6-} 271 (D_{5h})		0.0	16.04	17.81	1.77		
$C_{50}Cl_{10}$ (D_{5h})	$^1A_1'$		−6.92	−3.85	3.07	3.04	
C_{60} (I_h)			−5.99	−3.22	2.77	2.51 (2.67)[e]	

[a] The isomer numbering system for C_{50} follows ref 4. [b] Relative energy with respect to the D_3 singlet. [c] Its HOMO is $13a_1'$, and LUMO is $5a_2'$. [d] Its HOMO is $5a_2'$, and LUMO is $13a_1'$. [d] at B3LYP/6-31+G*// B3LYP/6-31G* level of theory. [e] Experimental values.

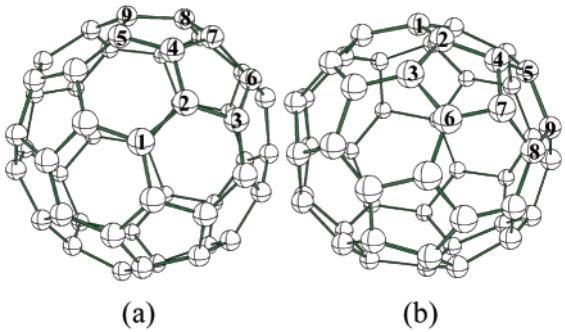

Figure 1. Geometry of C_{50} (D_3): (a) top view and (b) side view. The independent carbon atoms are numbered.

Table 2. Calculated Pyramidalization Angles θ_P (°) for C_{50}^q (q = 0, 2−, 6−; D_{5h} and D_3), $C_{50}Cl_{10}$ (D_{5h}) and C_{60} (I_h)

entity	C1	C2	C3	C4	C5	C6	C7	C8	C9
C_{50} (D_{5h}) (B)	10.7	12.5	12.8	15.5					
C_{50}^{2-} (D_{5h})	11.2	12.3	12.3	16.4					
C_{50}^{6-} (D_{5h})	12.6	10.6	11.1	19.4					
$C_{50}Cl_{10}$ (D_{5h})	12.2	10.2	9.4						
C_{50} (D_3)	9.6	12.5	11.8	14.0	12.6	13.3	15.2	12.5	12.2
C_{50}^{2-} (D_3)	9.7	11.4	12.1	16.8	11.6	12.7	14.5	13.1	11.8
C_{50}^{6-} (D_3)	9.0	11.4	11.2	16.5	11.5	11.1	18.6	12.0	12.2
C_{60} (I_h)	11.6								

The optimized structure of C_{50} (D_3) is shown in Figure 1; the B3LYP/6-31G* bond lengths are presented in Supporting Information Table 2. Due to the large HOMO−LUMO gap predicted for its ^1A ground state, no further attention has been paid to electronically excited states of this isomer. On the other hand, for the C_{50} (D_{5h}) isomer, a total of three low-lying states were investigated, i.e., two $^1A_1'$ singlet states and a $^3A_2'$ triplet state. Figure 2 depicts the geometry of neutral C_{50} (D_{5h}), and the optimized geometric parameters and relative energies of these electronic states are listed in Supporting Information Table 3.

The two $^1A_1'$ singlets of D_{5h} C_{50} differ in the occupancy of the frontier orbitals. In the $^1A_1'$ (A) state,[26] the highest occupied molecular orbital (HOMO) is the $13a_1'$ MO; the lowest unoccupied molecular orbital (LUMO) is $5a_2'$ (shown schematically in Figure 3). The HOMO and LUMO are reversed ($5a_2'$ and $13a_1'$, respectively) in the $^1A_1'$ (B) state.[25] Both the $5a_2'$ and $13a_1'$ MOs are singly occupied in the triplet $^3A_2'$ state. At the B3LYP/6-31G* level, the $^1A_1'$ (B) state is 3.3 and 4.5 kcal/mol lower in energy than the $^1A_1'$ (A) state and the $^3A_2'$ state, respectively. In addition, the HOMO−LUMO gaps of C_{50} (D_{5h}) in singlets are quite small, 1.27 and 1.37 eV for the $^1A_1'$ (A) and $^1A_1'$ (B) states, respectively. Closer inspection shows, however, that D_{5h} C_{50} has no diradical character, as indicated by zero value of S^2 in the unrestricted broken-symmetry DFT calculations and by nearly zero occupation of the LUMO orbital in the CASSCF(2,2)/6-31G*//B3LYP/6-31G* computations.[27]

Both the HOMO and LUMO coefficients of C_{50} (D_{5h}) are distributed around the equatorial pentagon−pentagon annulations (Figure 3). Thus, the pentalene-like fusions of C_{50} (D_{5h}) should function as active sites in chemical reactions. This explains why the Cl atoms in $C_{50}Cl_{10}$ are bound to the equatorial

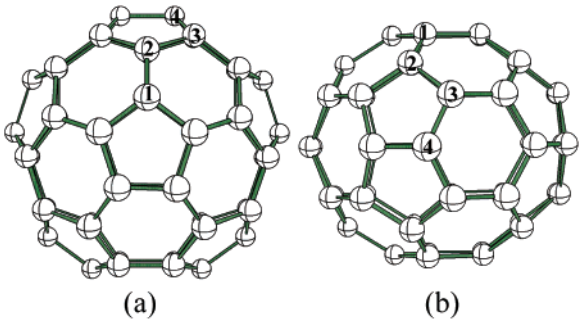

Figure 2. Geometry of C_{50} (D_{5h}) (a) top view, (b) side view. The independent carbon atoms are numbered.

Table 3. B3LYP/6-31G* Electronic Properties of Dimers of C_{50} (D_{5h})

entity	E_{dimer} [a] (kcal/mol)	E_{HOMO} (eV)	E_{LUMO} (eV)	E_g [b] (eV)
[2+2]	−40.2	−5.62	−3.81	1.81
[2+4]	−17.3	−5.64	−3.80	1.84
[4+4]	−27.2	−5.80	−3.77	2.03
[2+2] (open)	−0.6	−5.64	−3.94	1.70

[a] Dimerization energies. [b] Energy gap between the HOMO and LUMO orbitals.

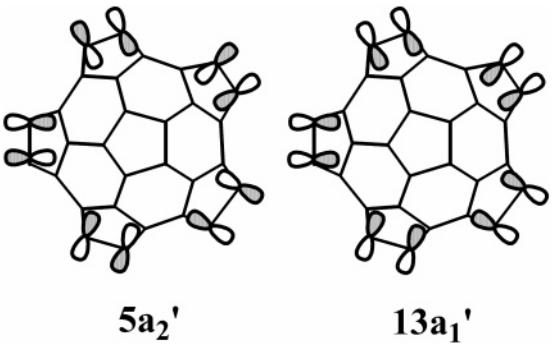

Figure 3. Schematic presentation of the frontier molecular orbitals of C_{50} (D_{5h}). (Top view along the C_5 axis).

Scheme 1

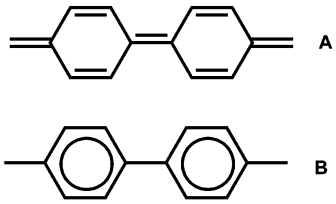

pentagon−pentagon fusions. Apparently, the $13a_1'$ MO is bonding, whereas the $5a'_2$ MO is antibonding for C−C bonds at the equatorial pentagon−pentagon fusions. The equatorial pentaphenyl belt within C_{50} (D_{5h}) can be regarded as being quinoid-like (Scheme 1A) in the $^1A_1'$ (A) state and benzene-like (Scheme 1B) in the $^1A_1'$ (B) state. This accounts for the structural difference between the two D_{5h} singlet states, i.e., the C−C bonds at the pentagon−pentagon fusions (∼1.40 Å) in the $^1A_1'$ (A) state are shorter than those (∼1.47 Å) in the $^1A_1'$ (B) state. The lower energy of $^1A_1'$ (B) compared with $^1A_1'$ (A) indicates that the double CC bonds at the equatorial pentagon−pentagon fusions are not favorable.

Significant strain can be expected at the pentagon−pentagon fusion sites of the C_{50} molecules. In general, the magnitude of angle strain at a fullerene carbon atom can be expressed by the pyramidalization angle (θ_P), which is defined by the angle between the π-orbital and adjacent σ-bonds, minus 90°.[28] π-orbital axis vector (POAV) analysis of the B3LYP/6-31G* optimized geometry of C_{50} (D_3) and C_{50} (D_{5h}) B is summarized in Table 2. For C_{50} (D_{5h}) B, the θ_P at a C4 atom (i.e., pentagon−pentagon apex fusion) is 15.5°, much bigger than those (10.7°, 12.5°, and 12.8°) at the C1, C2, and C3 atoms. The angle between the p_π orbital at a C4 atom and its adjacent σ-bonds is around 105.5°, very close to tetrahedral. Accordingly, the p_π orbital at a C4 atom would behave to some extent like a dangling bond, resulting in kinetic instability of C_{50} (D_{5h}). Similarly, C4 and C7 atoms at the pentagon fusion in C_{50} (D_3) also have much larger θ_P values than other atoms (Table 2), and will thus tend to be active sites for addition reactions.

Both C_{50}(D_3) and C_{50} (D_{5h}) should attract electrons strongly. The predicted LUMO eigenvalues for C_{50} (D_3) (−3.74 eV) and C_{50} (D_{5h}) B (−4.17 eV) are more negative than that of C_{60} (−3.22 eV at the same level of theory). Indeed, the experimental electron affinity (EA) of C_{50} (∼3.35 eV[29]) is even higher than that of C_{60} (2.668 ± 0.008 eV[30]).

2. Monoanion C_{50}^-. Both D_3 and D_{5h} isomers were investigated for C_{50} mono-, di- and hexaanions. D_3 C_{50}^- is 6.9 kcal/mol higher in energy than the electronic ground state of the D_{5h} anion. C_{50}^- (D_{5h}) has two low-lying doublet states, $^2A_1'$ and $^2A_2'$ (Table 1). These are derived from the $^1A_1'$ (B) and $^1A_1'$ (A) states of neutral C_{50} (D_{5h}), respectively. These two doublet states are close in energy at B3LYP/6-31G*, with $^2A_1'$ lower in energy by 2.1 kcal/mol. Since the HOMO and LUMO of neutral C_{50} (D_{5h}) are mainly delocalized over the equatorial pentagon−pentagon fusions, the attachment of an additional electron to neutral C_{50} affects primarily the C−C bond lengths of the equatorial area rather than the C−C distances of the polar parts. (cf. Supporting Information Table 3). The extra electron in the D_3 C_{50} anion occupies the LUMO of neutral D_3 C_{50}, and is mainly located at the C4 atoms, thus shortening the bonds in which they are involved.

The B3LYP/6-31+G* adiabatic electron affinity **(**AEA**)** and vertical electron affinity (VEA) of neutral D_3 and D_{5h} (B) C_{50} are summarized in Table 1. The AEAs are 0.07−0.14 eV greater than the VEAs. The VEAs of C_{50} (D_3) and C_{50} (D_{5h}) B are 2.97 and 3.40 eV, respectively, the latter agrees perfectly with the experimental estimate of ∼3.35 eV.[29] Note that the computed (VEA 2.51 eV) and measured (2.668 ± 0.008 eV)[30] EA values of C_{60} agree well at this theoretical level. The very large EA of C_{50}, measured or predicted to be greater than C_{60}, is consistent with the enhanced intensity of C_{50}^- observed in the gas-phase experiments.[29]

3. Dianion $C_{50}^{2-}$and Hexaanion C_{50}^{6-}. The computed CC bond lengths and electronic properties of C_{50}^{2-} and C_{50}^{6-}, both in D_3 and D_{5h} symmetries, are listed in Supporting Information Tables 1−2 and Table 1. The C_{50}^{2-} ground state has D_{5h} symmetry; its D_3 isomer is 18.6 kcal/mol higher in energy. D_{5h} C_{50}^{2-} has much larger HOMO−LUMO gap (2.12 eV) than that of neutral C_{50} (1.37 eV), since the bonding LUMO orbital of C_{50} (D_{5h}) B is filled in the dianion. These results imply substantial kinetic stability for D_{5h} C_{50}^{2-} salts. Accordingly, the preparation of ionic X_2C_{50} or YC_{50} compounds (X = alkaline metals; Y = alkaline earth metals) seems likely. Preliminary results show that D_{5h} Mg@C_{50} is 27.6 kcal/mol more stable than its endohedral D_3 isomer, and has a HOMO−LUMO gap of 1.53 eV (Table 1). Though the reaction Mg + C_{50} (D_{5h}) → Mg@C_{50} (D_{5h}) is endothermic, the accommodation energy of 16.0 kcal/mol is relatively small. Note that a helium atom has been incorporated into the much small $C_{20}H_{20}$ (I_h) cage[31] and that the computed accommodation energy is 35.0 kcal/mol.[32]

The D_3 and D_{5h} C_{50} dianions can be reduced further to hexaanions without losing their high symmetries; D_3 C_{50}^{6-} is computed to be 6.0 kcal/mol lower in energy than its D_{5h} analogue. Both D_3 and D_{5h} hexanions have appreciable HOMO-LUMP gap energies (2.53 and 1.77 eV, respectively).

Table 2 lists the POAV analyses of C_{50}, C_{50}^{2-}, and C_{50}^{6-} based on the B3LYP/6-31G* optimized geometries. The pyramidalization angle (θ_P) at the pentagon fusions of C_{50} (C4 in the D_{5h} isomer and C4 and C7 in the D_3 isomer) are larger in the charged species; the θ_P at C4 in D_{5h} C_{50} increases from

(27) The $^1A_1'$ (B) state of C_{50} (D_{5h}) is 17.7 kcal/mol more stable than $^1A_1'$ (A) at the CAS(2,2)/6-31G*//B3LYP/6-31G* level.
(28) Haddon, R. C.; Scott, L. *Pure Appl. Chem.* **1986**, *58*, 137. (b) Haddon, R. C. *Science* **1993**, *261*, 1545.
(29) Kietzmann, H.; Rochow, R.; Gantefor, G.; Eberhardt, W.; Vietze, K.; Seifert, G.; Fowler, P. W. *Phys. Rev. Lett.* **1998**, *81*, 5378.
(30) Wang, X.-B.; Ding, C.-F.; Wang, L.-S. *J. Chem. Phys.* **1999**, *110*, 8217.
(31) Cross, R. J.; Saunders, M.; Prinzbach, H. *Org. Lett.* **1999**, *1*, 1479.
(32) Chen, Z.; Jiao, H.; Bühl, M.; Hirsch, A.; Thiel, W. *Theor. Chem. Acc.* **2001**, *106*, 352.

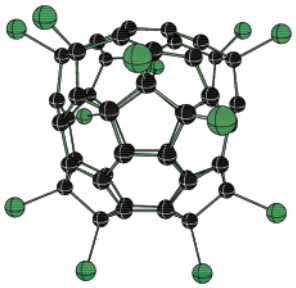

Figure 4. B3LYP/6-31G* optimized structure of $C_{50}Cl_{12}$ (D_3), in which the twelve Cl atoms are attached to the pentagon−pentagon apex fusions of C_{50} (D_3).

15.5° for the neutral to 19.7° for the hexaanion, while the θ_P's at C4 and C7 in D_3 C_{50} increase from 14.0° and 15.2° to 16.5° and 18.6°, respectively. The negative charges are mainly delocalized over the pentagon−pentagon fusions; hence, these are active sites for further reactions. For example, the large electron density at the C4 atoms of the D_{5h} isomer results in sp^3 hybridization and a large pyramidalization angle (19.7°) in the hexaanion. The decaanion C_{50}^{10-} has lone pairs of electrons localized at each C4-type atom.

Binding 10 atoms such as H and Cl to C4 atoms releases much of the strain of D_{5h} C_{50}; the hydrogenation and chlorination reaction energies (per H_2 or Cl_2) are highly exothermic (eqs 1−2; −50.9 and −50.7 kcal/mol, for $C_{50}H_{10}$ and $C_{50}Cl_{10}$, respectively). (For comparison, the hydrogenation energy of C_{20} to $C_{20}H_{20}$ is −61.9 kcal/mol per H_2). Accordingly, the D_{5h} C_{50} cage can function as a decavalent functional group, as evidenced by the preparation of the $C_{50}Cl_{10}$ compound for which ^{13}C NMR revealed only 4 types of chemically unequivalent C atoms.[15] Similarly, the D_3 C_{50} cage can provide up to 12 active sites (C4 and C7 positions) for addition reactions (eq 3−4). However, the D_3 isomer itself has 9 types of C atoms. Addition of only 10 Cl atoms onto the D_3 isomer would result in a $C_{50}Cl_{10}$ molecule with a much lower symmetry that has more than 9 types of C atoms. Hence, the D_3 isomer could not be the parent fullerene-[50] of $C_{50}Cl_{10}$ synthesized experimentally. Instead, addition of 12 Cl atoms onto the active sites of D_3 C_{50} gives rise to $C_{50}Cl_{12}$ (D_3) (Figure 4). Actually, $C_{50}Cl_{12}$ has already detected mass spectroscopically[33] using similar experimental conditions in which $C_{50}Cl_{10}$ (D_{5h}) is generated.[15] It might be possible to isolate $C_{50}Cl_{12}$ (D_3). The much lower hydrogenation (eq 3) and chlorination (eq 4) energies of D_3 C_{50} compared to D_{5h} C_{50} (eq 1 and 2) also indicate the smaller strain of the D_3 isomer

$$C_{50}\,(D_{5h}) + 5H_2 \rightarrow C_{50}H_{10}\,(D_{5h})$$
$$\Delta H\,(per\ H_2) = -50.9\ \text{kcal/mol} \quad (1)$$

$$C_{50}\,(D_{5h}) + 5Cl_2 \rightarrow C_{50}Cl_{10}\,(D_{5h})$$
$$\Delta H\,(per\ Cl_2) = -50.7\ \text{kcal/mol} \quad (2)$$

$$C_{50}\,(D_3) + 6H_2 \rightarrow C_{50}H_{12}\,(D_3)$$
$$\Delta H\,(per\ H_2) = -35.2\ \text{kcal/mol} \quad (3)$$

$$C_{50}\,(D_3) + 6Cl_2 \rightarrow C_{50}Cl_{12}\,(D_3)$$
$$\Delta H\,(per\ Cl_2) = -37.5\ \text{kcal/mol} \quad (4)$$

4. Dimerization of C_{50} (D_{5h}) and C_{50} (D_3). Macroscopic quantities of $C_{50}Cl_{10}$ (D_{5h}) have already been prepared.[15] However, bare C_{50} clusters would be subject to oligomerization and formation of carbon solids. Since C_{50} (D_{5h}) is highly strained at the equatorial pentagon−pentagon fusions, it is reasonable to assume that dimerization of C_{50} would occur readily at these pentagon−pentagon junctions. Four possible dimerization modes are considered (Figure 5). The calculated dimerization energies and electronic properties for these dimers are listed in Table 3.

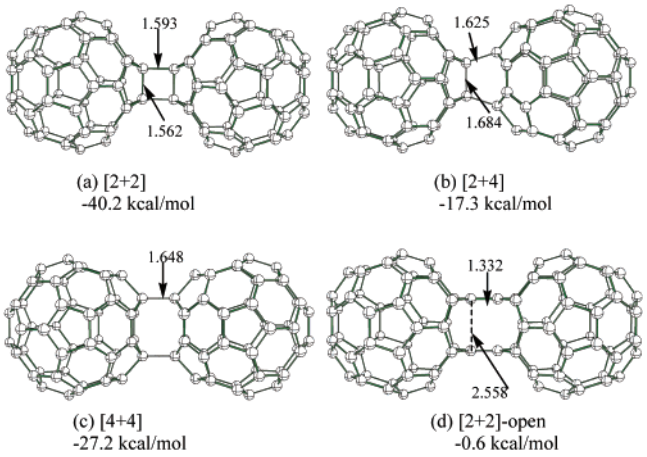

Figure 5. Four possible modes for the dimerization of C_{50} (D_{5h}). Key geometric parameters (bond lengths in Å) optimized at the B3LYP/6-31G* level and the dimerization energies are also given.

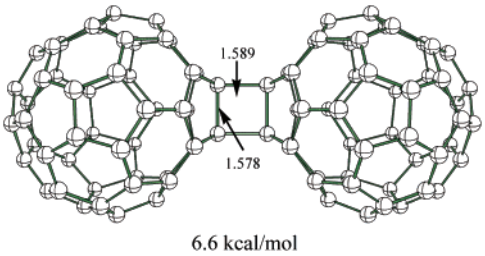

Figure 6. [2+2] dimer of C_{50} (D_3) (bond lengths in Å) and its dimerization energy.

The formal [2+2] dimerization mode (Figure 5a) is the most exothermic (−40.2 kcal/mol). The [4+4] and [4+2] exothermicities, −27.2 and −17.3 kcal/mol, respectively, are also substantial. In contrast, the [2+2]-open isomer (Figure 5d), which involves cleavage of the two formal C−C bonds of the closed dimer (Figure 5a) and the formation of two C═C bonds between two C_{50} cages, is relatively unfavorable.

The HOMO−LUMO gaps of the dimers are larger than that of C_{50} (D_{5h}). Further oligomerization is likely. As the active sites in C_{50} (D_{5h}) are the equatorial pentagon−pentagon fusions, the further oligomerization or polymerization of C_{50} (D_{5h}) might produce new two-dimensional layer structures. This topic deserves experimental and theoretical investigation.

The [2+2] dimerization of C_{50} (D_3) is shown in Figure 6. However, this reaction is predicted to be 6.6 kcal/mol endothermic, indicating that the [2+2] dimerization of C_{50} (D_3) is unfavorable. The resulting dimer has a LUMO−HOMO gap of 1.43 eV, ∼0.8 eV smaller than that of the monomer.

5. Structure and Electronic Properties of $C_{50}Cl_{10}$ (D_{5h}). $C_{50}Cl_{10}$ (D_{5h}) (Figure 7) has two conjugated C_{20} caps separated by five >C(Cl)−C(Cl)< groups. Its HOMO is the $17e_2''$ MO, and LUMO the $31e_1'$ MO. The B3LYP/6-31G* HOMO−LUMO gap (3.07 eV) is 1.7 eV greater than that of C_{50} (D_{5h}).

Furthermore, the LUMO eigenvalue of $C_{50}Cl_{10}$ (D_{5h}) is −3.85 eV, 0.6 eV lower than that of C_{60}. This suggests that $C_{50}Cl_{10}$

Table 4. Calculated[a] ^{13}C NMR Chemical Shifts (ppm) for D_{5h} and D_3 Symmetrical C_{50}, C_{50}^{2-}, C_{50}^{6-} as Well as $C_{50}Cl_{10}$ (D_{5h}), $C_{50}Cl_{12}$ (D_3) and C_{60} (I_h), and Comparison with the Available Experimental Data[b]

entity	symm	C1	C2	C3	C4	C5	C6	C7	C8	C9
C_{50}	D_3	143.5	143.3	152.2	170.8	140.0	155.4	177.0	156.3	142.4
C_{50}^{2-}	D_3	140.7	149.4	150.5	117.0	141.2	154.2	143.7	150.1	152.0
C_{50}^{6-}	D_3	159.1	165.1	148.2	168.0	158.9	156.9	146.9	152.7	147.0
C_{50}	D_{5h}	142.7	160.6	156.4	112.4					
C_{50}^{2-}	D_{5h}	144.3	156.7	157.1	175.4					
C_{50}^{6-}	D_{5h}	132.2	149.3	160.1	160.6					
C_{60}	I_h	142.5	(142.5[c])							
$C_{50}Cl_{10}$	D_{5h}	141.5 (143.2[d])	146.1 (146.8)[d]	163.6 (161.5)[d]	87.5 (88.7[d])					
$C_{50}Cl_{12}$	D_3	132.7	167.8	148.5	86.6	149.8	162.1	84.3	153.3	153.5

[a] See the text for details of the calculations; [b] experimental data are given in parentheses; [c] ref 19; [d] ref 15.

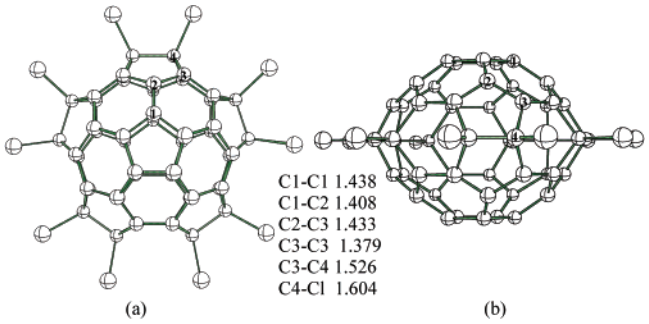

Figure 7. The B3LYP/6-31G* optimized geometry of $C_{50}Cl_{10}$ (D_{5h}) (a) top view, (b) side view.

(D_{5h}) should have a larger electron affinity than C_{60}. Indeed, the B3LYP/6-31+G* VEA of $C_{50}Cl_{10}$ is 3.04 eV, approaching that of D_{5h} C_{50} (3.40 eV) and by ~0.5 eV higher than that of C_{60} (~2.51 eV). It is known that halofullerenes, e.g., $C_{60}X_n$ (X = F, Cl, Br), are good electron-acceptors with possible photonic/photovoltaic applications.[34] Like its $C_{60}X_n$ analogues, similar application can be expected for $C_{50}Cl_{10}$.

6. Aromaticity of C_{50}, C_{50}^{2-}, C_{50}^{6-}, $C_{50}Cl_{10}$ (D_{5h}) and $C_{50}Cl_{12}$ (D_3). According to Hirsch's $2(N+1)^2$ electron counting rule for spherical molecules,[13] C_{50} is expected to be highly aromatic. Indeed, the NICS value at the cage center of the D_3 isomer (−40.3 ppm) is remarkably negative. Adding more electrons decreases the NICS values (dianion −16.6 ppm, hexaanion −14.7 ppm, and $C_{50}Cl_{12}$ −15.5 ppm). The same holds for the electronic state A of the D_{5h} isomer (NICS −32.4 ppm).[11] However, the more energetically favorable electronic state B of C_{50} (D_{5h}) is nonaromatic (NICS −2.7 ppm), but the NICS values are larger for the dianion (−33.7 ppm), the hexaanion (−11.1 ppm) and the $C_{50}Cl_{10}$ chlorine adduct (−17.5 ppm). The lower energy of the neutral D_3 isomer relative to the D_{5h} isomer is thus a synergy of the better electron delocalization and lower strain. The computed NICS values at the fullerene cages centers are equivalent to those measured experimentally via the endohedral ^3He chemical shifts.[35] Since the ^3He NMR chemical shifts are effective for characterizing fullerene structures,[36] the computed NICS values can help to distinguish the D_3 and D_{5h} isomers of neutral C_{50} in the gas phase.

7. Calculated ^{13}C NMR Chemical Shifts for $C_{50}Cl_{10}$, C_{50}, C_{50}^{2-}, C_{50}^{6-}, and $C_{50}Cl_{12}$. ^{13}C NMR chemical shifts are a powerful technique for determining fullerene structures.[37] The computed (GIAO-B3LYP/6-31G*) ^{13}C NMR chemical shifts for $C_{50}Cl_{10}$, C_{50}, C_{50}^{2-}, and C_{50}^{6-} are given in Table 4. For $C_{50}Cl_{10}$, the computed shifts, 141.5, 146.1, 163.6, and 87.5 ppm for C1, C2, C3, and C4 atoms, respectively, match experiments well (143.2, 146.8, 161.5, and 88.7 ppm). Thus, GIAO-B3LYP/6-31G* ^{13}C NMR chemical shifts predicted for C_{50}^{2-}, C_{50}^{6-} and their derivatives such as $C_{50}Cl_{12}$ (Table 6) should be reliable. Note that $C_{50}Cl_{12}$ (D_3) is a promising isolable species.

Table 5. Calculated IR-active Vibrational Wavenumbers (ν, cm^{-1}) and Intensities (I, km Mol^{-1}) for $C_{50}Cl_{10}$ (D_{5h}) at the B3LYP/6-31G* Level and Comparison with Experiment

	calcd.					calcd.			
	raw	scaled[a]		expt.[b]		raw	scaled[a]		expt.[b]
symm.	ν	ν	I	ν	symm.	ν	ν	I	ν
E_1'	1627	1594	0.8		E_1'	732	717	50.8	735(m)
A_2''	1600	1568	3.9	1558(w)	A_2''	707	693	13.3	694(w)
E_1'	1480	1450	2.1	1456(w)	E_1'	623	611	0.1	
A_2''	1461	1432	19.4	1433(w)	A_2''	620	608	11.0	609(w)
E_1'	1375	1347	8.6	1344(w)	E_1'	575	564	42.0	567(s)
E_1'	1358	1331	3.9	1324(w)	E_1'	481	471	0.3	
A_2''	1225	1201	0.4	1195(vw)	E_1'	452	443	34.8	450(s)
E_1'	1114	1092	1.4	1080(vw)	A_2''	404	396	0.9	
E_1'	1046	1025	85.6	1031(s)	E_1'	334	327	0.6	
A_2''	1011	991	13.6	997(w)	E_1'	293	287	5.5	
E_1'	1008	988	19.4	975(w)	E_1'	202	198	0.8	
E_1'	914	896	84.8	916(s)	A_2''	147	144	4.2	
E_1'	849	832	411.1	854(vs)	E_1'	127	124	0.3	
E_1'	786	770	38.6	777(m)					

[a] Scaled by a factor of 0.98. [b] ref 15.

8. Calculated IR- and Raman-Active Vibrational Modes and Intensities for $C_{50}Cl_{10}$ (D_{5h}). In principle, the 174 total vibrational modes of D_{5h} $C_{50}Cl_{10}$, $8A_2'' + 19\,E_1' + 11A_1' + 15\,E_1'' + 20\,E_2' + 7\,A_2' + 8\,A_1'' + 16\,E_2''$, give rise to 104 unique frequencies. Among them, the A_2'' and E_1' symmetry modes are IR active and A_1', E_2' and E_1'' irreducible representations are Raman active. Consequently, $C_{50}Cl_{10}$ ideally should display up to 27 unique wavenumbers in IR spectroscopic measurements and up to 46 unique wavenumbers in Raman measurements.

The computed IR frequencies (Tables 5−7) match the experimental data well.[15] Only several vibrational modes of E_1'

(33) Xie, S. Y.; Huang, R. B.; Deng, S. L.; Yu, L. J.; Zheng, L. S. *J. Phys. Chem. B* **2001**, *105*, 1734.
(34) Guldi, D. *Chem. Commun*. **2000**, 321.
(35) Bühl, M. *Chem. Eur. J*. **1998**, *4*, 734. (b) Bühl, M.; Hirsch, A. *Chem. Rev*. **2001**, *101*, 1153 and references therein.
(36) Saunders, M.; Jiménez-Vázquez, H. A.; Cross, R. J.; Mroczkowski, S.; Freedberg, D. L.; Anet, F. A. L. *Nature* **1994**, *367*, 256. (b) Saunders, M.; Jimenez-Vazquez H. A.; Cross, R. J.; Billups W. E.; Gesenberg, C.; Gonzalez, A.; Luo, W.; Haddon, R. C.; Diederich, F.; Herrmann, A. *J. Am. Chem. Soc*. **1995**, *117*, 9305. (c) Saunders, M.; Cross, R. J.; Jiménez-Vázquez, H. A.; Shimshi, R.; Khong, A. *Science* **1996**, *271*, 1693. (d) Shabtai, E.; Weitz, A.; Haddon, R. C.; Hoffman, R. E.; Rabinovitz, M.; Khong, A.; Cross, R. J.; Saunders, M.; Cheng, P. C.; Scott, L. T. *J. Am. Chem. Soc*. **1998**, *120*, 6389. (e) Wang, G. W.; Saunders, M.; Khong, A.; Cross, R. J. *J. Am. Chem. Soc*. **2000**, *122*, 3216.
(37) Jameson, C. J. *Annu. Rev. Phys. Chem*. **1996**, *47*, 135. (b) Wilson, M. A.; Pang, L. S. K.; Willett, G. D.; Fisher, K. J.; Dance, I. G. *Carbon* **1992**, *30*, 675.

Table 6. Calculated Raman-Active Vibrational Wavenumbers (ν, cm^{-1}) and Raman Scattering Activities (I, $Å^4$/amu) for $C_{50}Cl_{10}$ (D_{5h}) at the B3LYP/6-31G* Level and Comparison with Experiment

	calcd.					calcd.			
symm.	raw ν	scaled[a] ν	I	expt.[b] ν	symm.	raw ν	scaled[a] ν	I	expt.[b] ν
A_1'	1635	1602	165	1588(m)	A_1'	759	744	44	756(s)
E_2'	1598	1566	195	1567(s)	E_2'	754	739	14	
E_1''	1597	1565	27		E_2'	718	704	11	712(w)
E_2'	1504	1474	12	1490(w)	E_1''	703	689	1	
A_1'	1470	1441	557	1447(vs)	A_1'	676	662	40	670(s)
E_1''	1463	1434	8		E_2'	675	661	33	
E_2'	1376	1348	0.1		E_1''	621	609	0.1	
E_1''	1366	1339	10		E_2'	617	605	19	612(m)
E_1''	1348	1321	0.8		E_1''	586	574	0.1	
E_2'	1303	1277	37	1277(m)	A_1'	514	504	13	506(s)
A_1'	1239	1214	96	1214(m)	E_2'	509	499	4	
E_2'	1189	1165	27	1164(m)	E_1''	481	471	0.04	
E_1''	1175	1152	0.1		E_2'	448	439	5	
E_2'	1109	1087	4		A_1'	377	369	91	380(vs)
E_1''	1100	1078	19	1080(w)	E_2'	285	279	1	
A_1'	989	969	108	986(s)	E_1''	275	270	9	275(s)
E_2'	989	969	2		E_2'	235	230	14	

Table 7. TD-DFT Calculated Excitation Energies (λ), Oscillator Strengths (f), Degeneracy (D) and Transition Nature for the Optically Allowed Singlet Excitation States of $C_{50}Cl_{10}$ (D_{5h}) at the BP86/3-21G Level and Comparison with Experiment

	TD-DFT(BP86/3-21G)[a,b]					
sym.	λ (nm)	f	D	nature of transition	CI coefficient[c]	expt.[d] λ (nm)
A_2''	532.8	0.0183	1	$17e_1'' \rightarrow 31e_1'$	0.473	~530[f]
E_1'	451.2	0.0020	2	$11a_2' \rightarrow 31e_1'$	0.701	454.6[f]
E_1'	431.3	0.0453	2	$30e_2' \rightarrow 31e_1''$	0.437	433.8[e]
				$17e_2'' \rightarrow 18e_1''$	0.213	
A_2''	403.1	0.0001	1	$16e_1'' \rightarrow 31e_1'$	0.498	400.8[f]
E_1'	388.6	0.0001	2	$29e_2' \rightarrow 31e_1'$	0.474	
				$17e_2'' \rightarrow 18e_1''$	0.153	
A_2''	378.9	0.0155	1	$17e_2'' \rightarrow 31e_2'$	0.486	376.6[f]
E_1'	356.5	0.0551	2	$28e_2' \rightarrow 31e_1'$	0.340	356.5[e]
				$17e_2'' \rightarrow 18e_1''$	0.103	
				$29e_2' \rightarrow 31e_1'$	0.104	
				$30e_1' \rightarrow 31e_2'$	0.101	
				$30e_1' \rightarrow 20a_1'$	0.282	
A_2''	355.3	0.0009	1	$15e_1'' \rightarrow 31e_1'$	0.494	
E_1'	335.8	0.0422	2	$19a_1' \rightarrow 31e_1'$	0.101	334.0[e]
				$28e_2' \rightarrow 31e_1'$	0.336	
				$30e_1' \rightarrow 31e_2'$	0.196	
				$30e_1' \rightarrow 12a_2'$	0.188	
				$30e_1' \rightarrow 20a_1'$	0.113	
				$17e_1'' \rightarrow 13a_2''$	0.111	
				$17e_2'' \rightarrow 18e_1''$	0.186	
E_1'	332.4	0.0038	2	$19a_1' \rightarrow 31e_1'$	0.691	
A_2''	318.0	0.0059	1	$29e_1' \rightarrow 18e_1''$	0.230	322.0[e]
				$30e_1' \rightarrow 18e_1''$	0.422	
E_1'	317.5	0.0342	2	$30e_1' \rightarrow 31e_2'$	0.366	
				$30e_1' \rightarrow 20a_1'$	0.122	
				$30e_1' \rightarrow 12a_2'$	0.396	
E_1'	312.4	0.0303	2	$30e_2' \rightarrow 31e_2'$	0.418	
				$30e_1' \rightarrow 12a_2'$	0.288	
				$30e_1' \rightarrow 20a_1'$	0.203	
						238.5[e]

[a] B3LYP/6-31G* optimized geometry was used in the TD-DFT calculation. [b] The HOMO and LUMO of $C_{50}Cl_{10}$ (D_{5h}) are $17e_2''$ and $31e_1'$, respectively. [c] The transitions with coefficients larger than 0.100 are listed. [d] ref 15. [e] Data extracted from the UV−Vis spectrum.. [f] Data extracted from the fluorescence spectrum.

symmetry are computed to have considerable IR intensities, but all IR transitions involving A_2'' modes are predicted to be rather weak. The measured frequencies at 1031, 916, 854, 777, 735, 567, and 450 cm^{-1} with strong and moderate IR intensities are all due to vibrational modes of E_1' symmetry. The E_1' symmetry mode computed at 832(scaled)/849(unscaled) cm^{-1} has the largest intensity; The most intense measured peak is at 854 cm^{-1},[15] and is thus assigned to the E_1' mode, which involves the coupling of the asymmetric C−Cl stretching and deformation of C_{20} caps. Similarly, the other experimental IR peaks can be assigned unambiguously (Table 5).

Nineteen Raman spectral lines were observed for $C_{50}Cl_{10}$ (Table 6) experimentally, fewer than the expected total of 46 unique Raman-active vibrations. The agreement with the computed frequencies in Table 8 shows that all these experimentally observed Raman spectral lines are due to fundamental vibrations. Most of the observed Raman spectral lines with strong signals arise from A_1' vibrational modes. The observed strong peak at 1567 cm^{-1} and its shoulder at 1588 cm^{-1} are ascribed to C−C stretching modes with E_2' and A_1' symmetries, respectively. Another very strong peak at 1447 cm^{-1} is due to a symmetric C−C stretching mode of A_1' symmetry. Table 6 gives further details of the assignments of the experimental Raman spectral lines and the symmetry categories of their corresponding vibrational modes. The computed Raman-active frequencies (scaled) agree well with the experimental data; the largest deviation is 30 cm^{-1} for the E_2' mode (experiment 934 cm^{-1}, theoretical 904 cm^{-1} (scaled)). However, the agreement with experiment can be improved further by scaling the wavenumbers higher than 1000 cm^{-1} by 0.98. A similar technique was employed in the theoretical prediction of IR vibrational spectra of C_{70}.[22]

9. TD-DFT Study of the Excited States of $C_{50}Cl_{10}$ (D_{5h}). TD-DFT calculations at BP86/3-21G on the B3LYP/6-31G* optimized geometry of $C_{50}Cl_{10}$ show that excited state E_1' (356.5 nm) (out of 100 excited states) has the largest oscillator strengths of 0.0551. Table 7 lists all excited states with nonzero oscillator strengths, their corresponding excitation energies and transition nature. The lowest transition (596.5 nm, degeneracy = 2) from the HOMO ($17e_2''$) to the LUMO ($31e_1'$) is optically forbidden. The first optically allowed transition (532.8 nm) is from HOMO-1 ($17e_1''$) to LUMO ($31e_1'$), which corresponds to the optical gap of $C_{50}Cl_{10}$. In the UV−vis experiment on $C_{50}Cl_{10}$, five absorption bands with substantial intensities were observed centering at 433.8, 356.5, 334.0, 322.0, and 238.5 nm, respectively.[15] Thus, the predicted four E_1' states with excitation energies 431.3, 356.5, 335.8, and 317.5 nm coincide with the experimental data very well (indeed better than expected for TD-DFT calculations with the small 3-21G basis set[38]). Note that these assignments refer to the UV transitions with the highest computed intensity in the given energy region.

Concluding Remarks

A systematic density functional study has been performed on the electronic and spectroscopic properties of C_{50}, its anions, and the $C_{50}Cl_{10}$ and $C_{50}Cl_{12}$ derivatives. The D_3 and D_{5h} isomers are most favorable energetically for C_{50}. Due to the higher aromaticity and lower strain, the D_3 isomer is the ground state of C_{50} fullerene. Both D_3 and D_{5h} C_{50} have high electron affinities and can be reduced easily. The unstable fused pentagon structures makes C_{50} chemically labile; hence, C_{50} tends to add Cl_2, to dimerize, and to polymerize. The active sites in both D_3 and D_{5h} C_{50} are the pentagon−pentagon fusions; thus D_3 $C_{50}Cl_{12}$ and D_{5h} $C_{50}Cl_{10}$, in which such sites are saturated by

(38) The experimental optical absorption spectra of C_{60} and $C_{59}N^+$ were also reproduced very well at TD-BP86/3-21G. See Xie, R. H.; Bryant, G. W.; Sun, G.; Nicklaus, M. C.; Heringer, D.; Frauenheim, Th.; Manaa, M. R.; Smith, V. H., Jr.; Araki, Y.; Ito, O. *J. Chem. Phys.* **2004**, *120*, 5133.

chlorine atoms, are expected to be stable derivatives. The successful preparation, isolation and characterization of D_{5h} $C_{50}Cl_{10}$ prompts searches for D_3 $C_{50}Cl_{12}$, and further investigations on smaller fullerene chemistry.

Acknowledgment. This work was supported in China by NSF Grants No. 20021002, 20203013, 90206038, and 20023001, MOE Grant No. 20010384005, the Fok Ying-Tung Education Foundation, the MOST Grant No.2002CCA01600, the NSF of Fujian Province (Grants No. E0210001 and 2002F010), as well in USA by NSF Grant CHE-0209857 and in Germany by Alexander von Humboldt Stiftung (Z.C.).

Note Added in Proof: A paper titled "Density functional studies on the optical excitation and absorption spectra $C_{50}Cl_{10}$" was published on August 15, 2004, see Xie, R. H.; Bryant, G. W.; Cheung, C. F.; Smith, V. H., Jr.; Zhao, J. *J. Chem. Phys.* **2004**, *121*, 2849.

Supporting Information Available: Heats of formation for all possible C_{50} fullerene isomers, the structures of the six most stable C_{50} isomers at MNDO level, and the B3LYP/6-31G* optimized bond lengths of $C_{50}(D_3)$, $C_{50}(D_{5h})$ and their anions. This material is available free of charge via the Internet at http://pubs.acs.org..

JA046725A